Applied Magnetic Resonance (2020) 51:1093–1101
https://doi.org/10.1007/s00723-020-01259-1

Applied
Magnetic Resonance

ORIGINAL PAPER

Dielectric-Backed Aperture Resonators for X-band Depth-Limited in Vivo EPR Nail Dosimetry

Oleg Grinberg[1] · Jason W. Sidabras[3,4] · Dmitriy Tipikin[1] · Vladimir Krymov[1] · Steven G. Swarts[2] · Harold M. Swartz[1]

Received: 24 June 2020 / Revised: 18 August 2020 / Published online: 25 September 2020

Abstract

A new resonant geometry for X-band in vivo electron paramagnetic resonance (EPR) nail dosimetry has been developed, fabricated, and tested. The dielectric-backed aperture resonator (DAR) was specifically designed for depth-limited surface spectroscopy. The DAR improves EPR sensitivity of surface samples with sub-millimeter thicknesses by at least a factor of 20 compared to other aperture resonator designs. The increase in EPR sensitivity was achieved using a non-resonant dielectric slab which is placed on the aperture inside the cavity. The dielectric slab provides an increased microwave magnetic field, while minimizing the problematic resonance conditions of the aperture. It has been shown that the DAR provides sufficient sensitivity to make biologically-relevant measurements both in vitro and in vivo. This work demonstrates that in vivo tests with an equivalent dosimetry sensitivity of approximately 1.4 Gy are feasible. Plausible ways to further increase the sensitivity are discussed, such as, the introduction and simulations of a DAR based on a semi-spherical TE_{011} geometry.

1 Introduction

There is a need for rapid screening methods to assess for the exposure to ionizing radiation after an incident in which clinically-significant doses may have occurred. These methods are essential to guide efficient treatments based on an individual's radiation dose in the range that could lead to acute radiation syndrome [1–3]. Rapid

✉ Oleg Grinberg
oleggrinb@gmail.com

1 Geisel School of Medicine at Dartmouth, Hanover, NH 03755, USA

2 Department of Radiation Oncology, University of Florida, Gainesville, FL 32610, USA

3 Department of Biophysics, Medical College of Wisconsin, Milwaukee, WI 53211, USA

4 EPR Research Group, Max Planck for Chemical Energy Conversion, 45468 Mülheim an der Ruhr, Germany

screening methods must provide the ability to triage large populations quickly, be minimally invasive, and identify individuals who may have received exposures of 2 Gy or more. Significant effort has been devoted to develop electron paramagnetic resonance (EPR) as a technique that would provide retrospective dosimetry screening [4–6]. Teeth, fingernails, and toenails have been demonstrated as viable in vitro and in vivo EPR dosimetry assays, providing a dose estimate based on a radiation-induced EPR signal (RIS) that reflects the extent of exposure to ionizing radiation [7–9]. We focus this work on fingernail and toenail assays, while the methods provided here are also feasible on tooth measurements with little modification.

The technical approach of in vitro nail dosimetry methods is based on the use of X-band (9.5 GHz) or Q-band (35 GHz) EPR spectroscopy [8, 10]. With in vitro methods, clipped nail samples are taken on-site, stored at − 20 °C, and shipped to a facility were measurements are performed and a dose estimate is predicted. However, the clipping process for in vitro nail dosimetry creates a series of mechanically-induced signals (MIS) which complicate the dose estimate process [11].

Therefore, an entirely non-invasive in vivo nail dosimetry approach is desired. Such an approach allows: (1) an on-site dose distribution assessments through measurement of nails in both hands and both feet, (2) a radiation-induced EPR signal that is specific and linearly related to the dose of ionizing radiation and, in particular, is not affected by concurrent trauma or pre-existing conditions, (3) avoids any MIS generated by a clipping nails process, and (4) does not involve complex sample storage or limited, repeat, on-site measurements.

One challenge of in vivo measurement is the presence of live tissue in close proximity to the nails that cause significant losses and degrade resonator efficiency. Current L-band (1.2 GHz) approaches minimize the dielectric losses, but do not provided the desired sensitivity for nail dosimetry. By choosing an operating frequency at X-band, the EPR signal intensity is increased with frequency if there are no frequency dependent losses. To diminish the losses of the surrounding tissue, in vivo nail dosimetry requires the development of resonant geometries that limit the region-of-interest to only within the thickness of the much less lossy nail plate.

One such resonator is the aperture resonator, which was introduced by Ikeya et al. for X-band in vivo tooth dosimetry [12, 13]. The aperture resonator is described as a rectangular TE_{102} cavity with an aperture, either a hole or slot, cut in the far wall, illustrated in Fig. 1a. The sample is placed on the aperture where

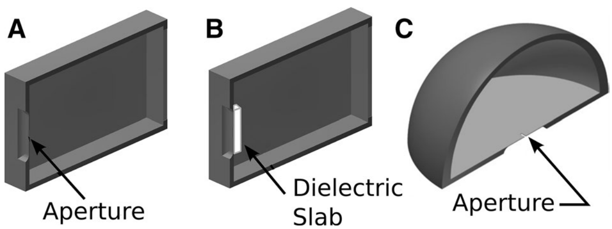

Fig. 1 Resonator geometries: **a** Rectangular TE_{102} based Aperture Resonator via Ikeya et al., **b** Dielectric-Backed Aperture Resonator, and **c** Semi-Spherical TE_{011} Aperture Resonator, which also can be dielectric-backed

an evanescent wave couples the spin system to the resonator. The power transmission through a thin-walled aperture in a flat conducting screen has been extensively investigated by Bethe [14] and in a series of publications by Harold Levine et al. [15, 16]. Although the aperture resonator described by Ikeya et al. looked very promising for nail in vivo EPR dosimetry, we have recognized during our investigations that these aperture resonators do not provide sufficient sensitivity for in vivo EPR nail dosimetry.

EPR signal enhancement through small aperture has received a growing interest since successful experiments by Ebbesen [17]. Several different aperture modifications have been suggested to maximize microwave magnetic field strength at the aperture [18–20]. Increase of microwave transmission through an aperture was shown in a number of studies [21–23] by designing the aperture to operate at resonance. Such designs are challenging due to significant changes in the aperture resonance condition under various sample-loading conditions, resulting in inconsistent EPR signal intensities.

In this work, we present a new aperture resonator geometry based on Ikea et al. geometry: the dielectric-backed aperture resonator (DAR), illustrated in Fig. 1b. It was recognized that EPR sensitivity could be improved by increasing the effective microwave magnetic field at the aperture using a non-resonant dielectric slab. The dielectric slab provides an increased microwave magnetic field at the aperture, and therefore the sample, while minimizing the sensitivity of the aperture resonance to the load conditions. This work also introduces a DAR semi-spherical TE_{011} geometry, illustrated in Fig. 1c. The semi-spherical TE_{011} geometry is attractive due to twice the incident microwave magnetic field at the aperture for a fixed input power. For clarity, illustrated in Fig. 2a is the microwave magnetic field profile of a rectangular TE_{102} aperture resonator, where the max microwave magnetic field is in the center of the cavity while the aperture is on a sidewall. However, the semi-spherical TE_{011} geometry has the aperture on the semi-spherical plane where the microwave magnetic field is maximum, illustrated in Fig. 2b. The semi-spherical TE_{011} geometry is modified by two “flat” regions to align the microwave magnetic field. In both configurations the dielectric is placed over the aperture to create the DAR geometry.

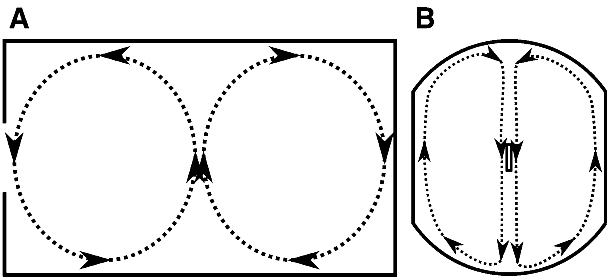

Fig. 2 Illustration of the microwave magnetic field profile for two aperture resonator geometries. **a** The rectangular TE_{102} and **b** semi-spherical TE_{011}

2 Methods

Finite-element simulations were performed with Ansys High Frequency Structure Simulator (HFSS; Version 15.0) on a Windows 7 64-bit Lenovo Think Vantage laptop. Both eigen-mode, where the solution is based on lowest energy states, and driven-mode, where power is coupled into a port, were used in the design process. Typical simulation time was about 30 min. A series of aperture resonator and DAR geometries have been designed, evaluated, and optimized by HFSS. Designs were chosen based on the signal intensity of unsaturable samples, Su, where the signal at critical coupling is calculated at constant microwave incident power using formulas derived by Mett et al. [24].

Resonator construction of the semi-spherical TE_{011} cavity and rectangular TE_{102} cavity has been made of copper bulk in an in-house machine shop. Rectangular TE_{102} cavity dimensions of $23.8 \times 43.6 \times 10.8$ mm^3 and semi-spherical TE_{011} of 23.1 (x-diameter) $\times$ 19.4 (z-dimension) mm, were chosen to provide a resonance frequency around 9.5 GHz. Design and construction of the DAR allows variation of several structural parameters such as the aperture and coupling iris dimensions, dielectric insert, and tuning mechanisms.

Particular attention to the flat aperture wall is required in fabrication of the DAR. Laser cutting (Potomac Photonics, Baltimore MD) precisely creates an aperture slit in the center walls of a 0.2 mm copper foil to couple microwave fields into the sample. A series of aperture walls with different aperture lengths (from 4 to 8 mm, 0.2 mm step) and 1 mm width were available for testing. These foils were silver plated (Specialized Plating Inc., Haverhill NH) to prevent the unwanted signal from copper oxide that was found to appear overtime. Field modulation coils were matched for a Bruker spectrometer and wound using copper wire on a custom saddle coil holder. Scotch tape is used affix the different dielectric geometries on the aperture inside the desired cavity. Dielectric slabs of various materials, such as E2000 SERIES, Sapphire, TiO_2, and $KTaO_3$, were all used for HFSS simulations and optimization. Bench tests used a $5 \times 10 \times 0.5$ mm slab of $KTaO_3$ ($\varepsilon_r = 372$, tan $\delta = 0.004$).

Three experimental models are used to evaluate the performance of fabricated resonators. The first is to create an in vitro fingernail model made of films with singlet EPR signals backed by a tissue equivalent polyacrylamide gel block (PAA) [25]. It was found that DuPont (Wilmington, DE) Kapton adhesive thin films, Kapton25 (0.0025″) and Kapton35 (0.0035″), have a stable repeatable EPR singlet with a 12.5 Gy and 35 Gy, respectively, equivalent radiation induced signal (RIS) dosage in a nail plate. Experiments were performed with one or three Kapton films attached to bleached printer paper to simulate a full nail thickness of 0.8–1 mm. Secondly, depth sensitivity measurements were performed by placing a Rogers 5880 PC board material (equivalent to 90 Gy RIS signal; 0.25 mm thickness) at fixed distance with bleached paper spacers on a finger model [26]. Lastly, in vivo tests were performed using a healthy volunteer nail with surface-attached Kapton films. The volunteer's finger was held in a custom-made 3D printed holder.

EPR spectra were acquired using Bruker Elexsys X-band spectrometer with a time constant of 10 ms, sweep time of 10 s, and field scans of 150 G. The amplitude of the 100 kHz field modulation, approximately 6 G, was chosen for maximum EPR signal intensity. A weak signal standard using the Bruker dosimetry reference standard ($g = 1.998$) was affix to the aperture wall. Current configurations did not use the reference signal as an intensity standard due to the replacement of aperture walls. Instead, the standard was used to enable proper microwave magnetic field positioning. The noise value was calculated as two standard deviations (noise SD) from the mean, which accounts for 95.45% of noise (assuming normal distribution). Noise SD was defined in off resonance of the EPR spectra chosen voluntarily by eye. To characterize resonator performance the term "RIS equivalent signal sensitivity" was introduced, which illustrates minimum dose that could be detected with SNR = 1 for each measurement.

3 Results

3.1 Simulation Results

Five cavity geometries were simulated to gain intuition on the relationship between cavity microwave magnetic field and the aperture geometry. Simulations predict that EPR signal intensity achieves a maximum value at a certain aperture size that reflects optimal product of the Q value times the filling factor due to increase of microwave magnetic field when aperture length increases, as shown in Fig. 3. A Cylindrical TM_{010} with a rectangular aperture of 1 mm width and varied length (filled triangle) and Cylindrical TE_{011} with a rectangular aperture of 1 mm width and varied length (filled circle) were simulated and found to have a maximum EPR signal intensity of 0.25 V and 0.21 V, respectively. Additionally, a rectangular TE_{102} with a circular aperture of varied diameter (filled square) was simulated and found to have a maximum EPR signal intensity of 0.24 V. The base geometry of this work, a Rectangular TE_{102} with a rectangular aperture with a 1 mm width and varied

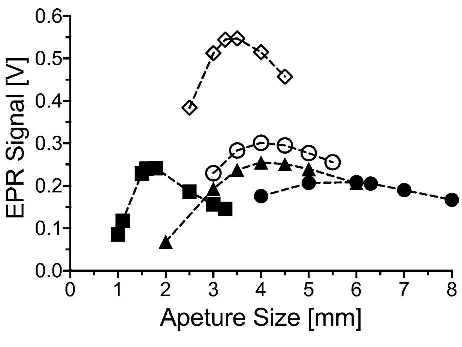

Fig. 3 Simulated EPR signal intensity versus aperture length for various resonator geometries without dielectric slabs. Rectangular TE_{102} rectangular aperture 1 mm width (opened circle), Semi-Spherical TE_{011} rectangular aperture 1 mm width (opened diamond), Rectangular TE_{102} circular aperture (filled square), Cylindrical TM_{010} rectangular aperture 1 mm width (filled triangle), Cylindrical TE_{011} rectangular aperture 1 mm width (filled circle)

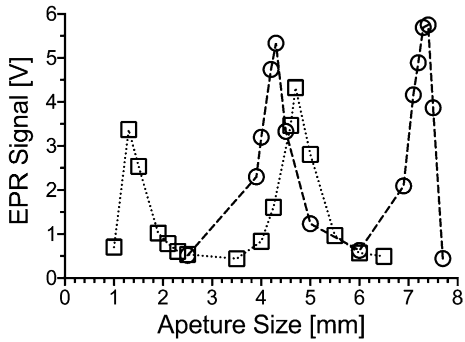

Fig. 4 Simulated EPR signal intensity versus aperture length for Dielectric-Backed Aperture Resonator Rectangular TE_{102} with aperture thickness of 0.5 mm (opened circle) and 1.0 mm (opened square)

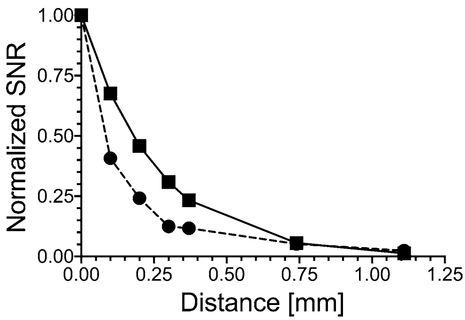

Fig. 5 Depth sensitivity data of a DAR Rectangular TE_{102} with an aperture dimension of 1.0×6.1 mm. Simulated (solid) and measured (dashed) depth sensitivity data is shown

length (opened circle) was simulated. A maximum EPR signal intensity of 0.30 V calculated was found at an iris length of 4 mm. Finally, a semi-spherical TE_{011} with a rectangular aperture with a 1 mm aperture width and varied length (opened diamond) was simulated. A maximum EPR signal intensity of 0.55 V was found at an iris length of 3.5 mm.

Significant increase in EPR signal intensity was calculated by placing a dielectric slab of $KTaO_3$, as shown in Fig. 1b, creating the DAR from a Rectangular TE_{102} with a rectangular aperture at two slab thicknesses of 0.5 mm (opened circle) and 1.0 mm (opened square). The aperture lengths were then varied and plotted in Fig. 4. Two resonance peaks are shown. Experimental measurements support the illustrated resonance phenomenon. However, the experimentally observed optimal aperture sizes slightly differ from predicted from simulations by approximately 1 mm. The trend suggests the discrepancy is due to the aperture thickness of 0.2 mm used in the experiments. This thickness was chosen to minimized depth sensitivity, as shown in Fig. 5, comparing the DAR with an aperture thickness of 0.5 mm (simulation) and 0.2 mm (measurement).

3.2 In Vitro Results

Using the PAA finger model and Rogers 5880 PC board material, a depth sensitivity profile was completed for an experimentally optimal DAR Rectangular TE_{102} with

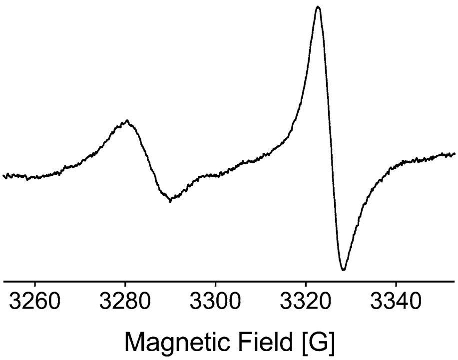

Fig. 6 EPR in vitro measurements using the polyacrylamide finger model with three Kapton25 films and bleached printer paper for a total thickness of 0.8 mm. Signal is shown at 3285G with Bruker standard at 3327G

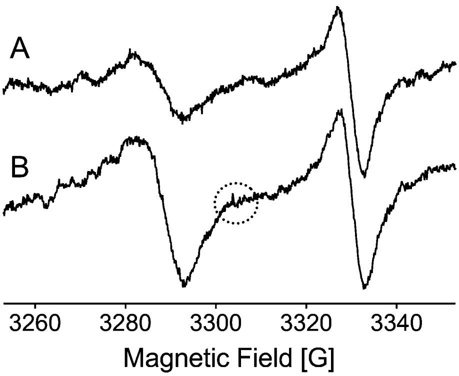

Fig. 7 EPR in vivo measurements on a healthy volunteer with **a** Kapton25 film (15 Gy equivalent) and **b** Kapton35 (35 Gy equivalent) film placed on a nail. Signal is shown at 3290G with Bruker standard at 3332G. Physiological noise is highlighted

an aperture dimension of 1.0×6.1 mm^2. The PC board material was placed between 0.1 mm PTFE sheets and moved at interval steps. The EPR signal intensity was recorded and plotted in Fig. 5. The EPR signal intensity was normalized at 0 mm and compared to Ansys HFSS data (solid). Good agreement is shown.

Finally, using the PAA finger model and three Kapton25 films placed on bleached copy paper (total thickness of 0.8 mm) a spectrum with an RIS equivalent signal of 45 Gy was measured and is shown in Fig. 6. A signal-to-noise of 63 is calculated, which corresponds to a 1.4 Gy RIS equivalent signal sensitivity.

3.3 In Vivo Results

The in vivo results were performed by placing Kapton25 and Kapton35 films directly on the fingernails of healthy volunteers and measuring the EPR signal intensity. Using these spectra a signal-to-noise of 55 was calculated, which corresponds to a RIS equivalent signal sensitivity of 1.2 Gy and 1.37 Gy, respectively. Results for Kapton25 and Kapton35 are shown in Fig. 7a and b. The in vivo tests have shown the influence of physiological motions (finger trembling, heartbeats, breathing, etc.) on spectra quality. A larger time constant of 163.84 ms was used to partially offset effect of these motions on the spectra.

4 Conclusions and Discussion

Simulations show that placement of a slab of dielectric material ($KTaO_3$) at the aperture inside the rectangular TE_{102} cavity results in a 20-fold increase in EPR signal intensity over a non-backed aperture configuration. The increase of the EPR signal arises as a result of increased microwave magnetic field strength at the aperture. Interesting to note is that the observed increase in microwave magnetic field strength at the aperture and sample, and minimization of sensitive aperture resonance conditions, are provided by the non-resonant dielectric slab. Unfortunately, dielectric slabs may have paramagnetic impurities that result in unwanted EPR signals. Care must be taken in selecting a pure dielectric source. Further improvements of signal-to-noise are expected by the implementation of a DAR semi-spherical TE_{011} geometry.

By focusing on depth-limited samples surrounded by lossy mediums, the DAR geometries may be of interest in other applications where the paramagnetic centers are limited to a shallow surface. For instance, the simplicity of the DAR resonator design may be advantageous in thin-film catalytic research or in vivo studies of melanin for melanoma research [27].

In this work, in vivo tests have shown that physiological motions do not significantly affect signal amplitude or regular noise. However, they often create spikes in the spectrum that could not be averaged during reasonable signal accumulations, as highlighted in Fig. 7. Although in vivo tests have shown effects of physiological motions and suggest necessity of a more robust finger holder, equivalent dosimetry sensitivity of approximately 1.4 Gy is demonstrated in the current resonator designs.

Acknowledgements This work is supported by Centers for Medical Countermeasures Against Radiation (CMCR) in the National Institute of Allergy and Infectious Diseases (NIAID) in the [Grant Number U19AI091173]; and the National Biomedical Electron Paramagnetic Resonance Center in the National Institute of Biomedical Imaging and Bioengineering (NIBIB) [Grant Number P41EB001980] of the National Institute of Health.

References

1. G.A. Alexander, H.M. Swartz, S.A. Amundson, W.F. Blakely, B. Buddemeier, B. Gallez, N. Dainiak, R.E. Goans, R.B. Hayes, P.C. Lowry, BiodosEPR-2006 meeting. Radiat. Meas. **42**, 972–996 (2007)
2. H.M. Swartz, B.B. Williams, A.B. Flood, Radiat. Environ. Biophys. **53**, 221–232 (2014)
3. D.J. Brenner, N.J. Chao, J.S. Greenberger, C. Guha, W.H. McBride, H.M. Swartz, J.P. Williams, Int. J. Radiat. Oncol. **92**(3), 504–505 (2015)
4. M.C.R. Symons, H. Chandra, J.I. Wyatt, Radiat. Prot. Dosim. **58**, 11–15 (1995)
5. B.G. Dalgarno, J.D. McClymont, Appl. Radiat. Isot. **40**, 1013–1020 (1989)
6. A. Romanyukha, F. Trompier, B. LeBlanc, C. Calas, I. Clairand, C.A. Mitchell, J.G. Smirniotopoulos, H.M. Swartz, Radiat. Meas. **42**, 1110–1113 (2007)
7. B.B. Williams, A.B. Flood, I. Salikhov, K. Kobayashi, R. Dong, K. Rychert, G. Du, W. Schreiber, H.M. Swartz, Radiat. Environ. Biophys. **53**(2), 335–346 (2014)
8. H. Xiaoming, S.G. Swarts, E. Demidenko, A.B. Flood, O. Grinberg, J. Gui, M. Mariani, S.D. Marsh, A.E. Ruuge, J.W. Sidabras, D. Tipikin, D.E. Wilcox, H.M. Swartz, Radiat. Prot. Dosim. **159**(1–4), 172–181 (2014)

9. N. Bahar, K. Roberts, F. Stabile, N. Mongillo, R.D. Decker, L.D. Wilson, Z. Husain, J. Contessa, B.B. Williams, A.B. Flood, H.M. Swartz, D.J. Carlson, SU-C-BRD-05. Med. Phys. **42**, 3192–3193 (2015)
10. A. Romanyukha, F. Trompier, R.A. Reyes, D.M. Christensen, C.J. Iddins, S.L. Sugarman, Radiat. Environ. Biophys. **53**(4), 755–762 (2014)
11. A. Marciniak, B. Ciesielski, A. Prawdzik-Dampc, Radiat. Prot. Dosim. **162**(1–2), 6–9 (2014)
12. M. Ikeya, M. Furusawa, Appl. Radiat. Isot. **40**(10–12), 845–850 (1989)
13. H. Ishii, M. Ikeya, Jpn. J. Appl. Phys. **29**(1–5), 871–875 (1990)
14. H.A. Bethe, Phys. Rev. **66**, 163–182 (1944)
15. H. Levine, J. Schwinger, Phys. Rev. **74**(8), 958–974 (1948)
16. H. Levine, J. Schwinger, Comm. Pure Appl. Math. **4**(3), 355–391 (1950)
17. T.W. Ebbesen, H.J. Lezec, H.F. Ghaemi, T. Thio, P.A. Wolff, Nature **391**, 667–669 (1998)
18. M.J. Lockyear, A.P. Hibbins, J.R. Sambles, Appl. Phys. Lett. **91**(25), 251106 (2007)
19. K. Aydin, A.O. Cakmak, L. Sahin, Z. Li, F. Bilotti, L. Vegni, E. Ozbay, Phys. Rev. Lett. **102**(1), 013904 (2009)
20. L. Scorrano, F. Bilotti, E. Ozbay, L. Vegni, Appl. Phys. A-Mater. **103**(3), 927–931 (2011)
21. F.Z. Yang, J.R. Sambles, Phys. Rev. Lett. **89**(6), 063901 (2002)
22. J.R. Suckling, J. Sambles, C.R. Lawrence, Phys. Rev. Lett. **95**(18), 187407 (2005)
23. J.R. Suckling, A.P. Hibbins, J.R. Sambles, C.R. Lawrence, New J. Phys. **7**(250), 1–11 (2005)
24. J.S. Hyde, J.W. Sidabras, R.R. Mett, in *Multifrequency Electron Paramagnetic Resonance: Theory and Applications*, ed. by S.K. Misra (Wiley, Hoboken, 2011) Chapt. 5.2
25. M.G. Bini, A. Ignesti, L. Millanta, R. Olmi, N. Rubino, R. Vanni, IEEE Trans. Bio-med. Eng. **31**(3), 317–322 (1984)
26. J.W. Sidabras, S.K. Varanasi, R.R. Mett, S.G. Swarts, H.M. Swartz, J.S. Hyde, Rev. Sci. Instrum. **85**, #104707 (2014)
27. C.M. Desmet, P. Danhier, S. Acciardo, P. Levêque, B. Gallez, Free Radic. Res. **53**(4), 405–410 (2019)